Industrial Crops & Products 251 (2026) 124155

Contents lists available at ScienceDirect

Industrial Crops & Products

journal homepage: www.elsevier.com/locate/indcrop

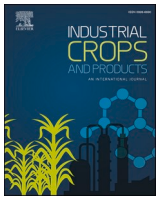

Interfacial enhancement of bamboo flour/poly(3-hydroxybutyrate-co-3-hydroxyvalerate) biocomposites enabled by synergistic treatment via delignification and PHBV-based coupling agent impregnation

Zhuoyu Lu [a], Nuoyan Ou [a], Lanying Lin [b], Kun Liu [a], Xiaolu Wu [a], Chuanshuang Hu [a,*], Jiangtao Xu [a], Yonghui Zhou [a,*], Mizi Fan [c]

[a] College of Future Biomass, South China Agricultural University, Guangzhou 510642, China
[b] Research Institute of Wood Industry, Chinese Academy of Forestry, Beijing 100091, China
[c] Department of Civil and Environmental Engineering, Brunel University of London, Kingston Lane, Uxbridge UB8 3PH, UK

ARTICLE INFO

Keywords:
Bamboo flour
Poly(3-hydroxybutyrate-co-3-hydroxyvalerate)
Composites
Interfacial enhancement

ABSTRACT

This paper presents a novel development of bamboo flour/poly(3-hydroxybutyrate-co-3-hydroxyvalerate) (PHBV) biocomposites with a particular focus on addressing the interfacial bonding through a synergistic treatment. The synergistic strategy involves the delignification of bamboo flour followed by impregnation of PHBV-based coupling agents synthesised in this work, including maleic anhydride (MA)-grafted PHBV (MA-*g*-PHBV), acrylic acid (AA) grafted-PHBV (AA-*g*-PHBV) and itaconic anhydride (IA) grafted-PHBV (IA-*g*-PHBV). Chemical structural analyses of bamboo flour suggested the removal of lignin and the possible interactions between surface hydroxyl groups and the introduced anhydride/carboxyl groups after the synergistic treatment. Microstructure analysis suggested the treated bamboo flour with increased surface roughness had better interfacial adhesion with PHBV matrix in the composites, which was further confirmed by their lower loss factor. The tensile strength and flexural strength of MA-*g*-PHBV modified delignified bamboo flour/PHBV composite were increased by 333.3% and 250.4% respectively, compared to those of the untreated counterpart. The improved interfacial bonding also resulted in the shift of composite failure mechanism from fibre pull-out to fibre breakage. The work provides a feasible and effective modification approach of lignocellulosic fibres for enhancing fibre-matrix interfacial bonding in biobased and biodegradable composites.

1. Introduction

Wood-plastic composites (WPCs) have undergone a speedy development in the last decade due to their environmental benefits, low life-cycle costs, and improved performance. This has led to rapid market growth and expansion in applications, including building and construction, automotive, consumer goods, packaging, etc (Wang et al., 2026; Chen et al., 2025). Currently, most commercially available WPCs employ non-degradable petroleum-based polymers such as polypropylene (PP), polyethylene (PE), and polyvinyl chloride (PVC) as the matrix. This reliance on petroleum-derived plastics presents significant challenges for recycling and reuse (Elsheikh et al., 2022; Bhattacharjee and Bajwa, 2018; Burgstaller and Renner, 2023). Furthermore, the disposal of WPC waste via landfilling or incineration can lead to the release of microplastics or harmful gases, posing potential risks to human health and the environment (Jung et al., 2025; Singh et al., 2023).

To address these issues, polyhydroxyalkanoates (PHAs) have emerged as a sustainable alternative to conventional polymer matrices. PHAs are microbially synthesised, fully biodegradable, and biocompatible, offering a green solution to the end-of-life management of WPCs. Among them, poly(3-hydroxybutyrate-co−3-hydroxyvalerate) (PHBV) is particularly promising, as it exhibits mechanical properties comparable to those of PP and has therefore been widely investigated as a matrix for WPCs (Farmahini-Farahani et al., 2017; Wu, 2014, 2013; Wu et al., 2017). Nevertheless, the abundance of hydroxyl groups on wood

* Corresponding authors.
E-mail addresses: cshu@scau.edu.cn (C. Hu), y.zhou@scau.edu.cn (Y. Zhou).

https://doi.org/10.1016/j.indcrop.2026.124155
Received 12 November 2025; Received in revised form 31 July 2026; Accepted 10 August 2026
Available online 14 August 2026

fibre surfaces imparts high polarity, resulting in poor adhesion with the non-polar PHBV matrix. Additionally, strong hydrogen bonding between fibres leads to agglomeration during melt blending, creating stress concentration defects that compromise composite performance (Rao et al., 2018; Zhang et al., 2018). To overcome these issues, fibre-matrix compatibility is commonly enhanced using single or combined modification strategies, including alkaline treatment, compatibilisers, silane or maleic coupling agents, which collectively improve the mechanical properties of WPCs (Frącz et al., 2021; Remila et al., 2024a; Nath et al., 2025). In addition, maximising the loadings of natural fibre in biodegradable WPCs is of great economical significance considering the much lower cost of natural fibre than bioplastics. Previous studies on PHBV-based WPCs have typically incorporated natural fibre at loadings of 30–40 wt% or lower, with relatively few reports investigating higher fibre contents of 50 wt% or above. High fibre loadings tend to exacerbate fibre agglomeration during processing, further degrading composite mechanical performance (Rao et al., 2018).

Coupling agent treatment is the most industrially feasible yet efficient modification strategy for enhancing interfacial adhesion in WPCs (Nath et al., 2025; Hwang et al., 2012). Among which, maleic anhydride (MA) is a commonly used grafting monomer, while several studies have also employed acrylic acid (AA) and itaconic anhydride (IA) as grafting monomers to synthesize coupling agents (Wu, 2014; Conti Silva et al., 2022). The macromolecular backbone (e.g. polylactic acid (PLA) and PHBV) of the coupling agent shares the same chemical nature as the composite matrix, ensuring excellent thermodynamic compatibility and molecular chain entanglement (Hao et al., 2021). On the other hand, the cyclic anhydride groups of MA and IA can undergo ring-opening during thermal processing to generate two carboxyl groups, while AA itself carries one carboxyl group. These carboxyl groups can react with the hydroxyl groups (-OH) on the surface of cellulosic fillers in WPCs, forming covalent bonds (Niwa et al., 2017).

In this study, bamboo flour (BF) was selected as the cellulosic filler in BF/PHBV biocomposites due to its excellent mechanical properties and abundance in southern China (Xu et al., 2021). Bearing the aim of enhancing the interfacial bonding between the high-loading bamboo flour and PHBV matrix, a synergistic treatment strategy involving delignification of BF followed by impregnation of PHBV-based coupling agents was developed (Fig. 1). The focus of the work was to reveal the physical and chemical structure variations of BF during the synergistic treatment, and the subsequent impact on the interfacial bonding of BF/PHBV biocomposites. Static and dynamic mechanical property and thermal stability were also determined to explore the interfacial structure-performance relationship of the biocomposites.

2. Materials and methods

2.1. Materials

Moso bamboo (*Phyllostachys edulis*), sourced from Hengyang, Hunan Province, China, were pulverised and sieved through a 40–60 mesh screen. The resulting bamboo flour was oven-dried at 105 °C for 24 h prior to use. PHBV (grades Y1000P granular, and Y1000 powder) was obtained from Tianan Biological Materials Ltd. (Zhejiang, China). Maleic anhydride (MA), acrylic acid (AA), sodium chlorite ($NaClO_2$), lubricant including 12-hydroxystearic acid and zinc stearate and initiator benzoyl peroxide (BPO) were purchased from Shanghai Macklin Biochemical Co., Ltd. (Shanghai, China). Itaconic anhydride (IA), diisopropylbenzene peroxide (DCP), and dichloromethane (DCM) were purchased from Shanghai Aladdin Biochemical Technology Co., Ltd. (Shanghai, China). All chemicals were of analytical grade and used without further purification.

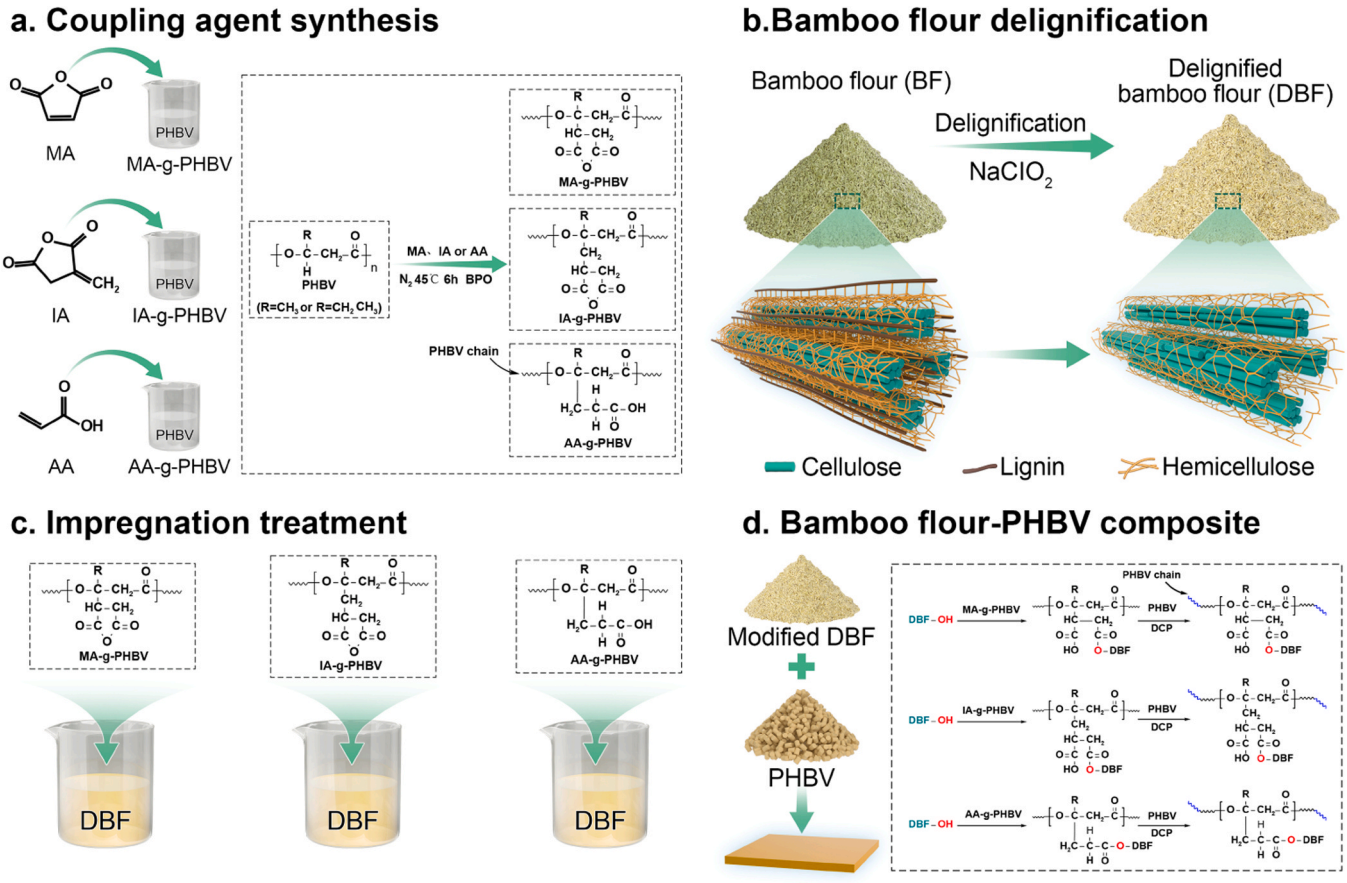

Fig. 1. Schematic illustration of preparation of BF-PHBV composites by applying the synergistic treatment.

2.2. Methods

2.2.1. Synthesis of PHBV-based coupling agents

The grafting of MA onto PHBV was performed under a nitrogen atmosphere as follows: 6 g PHBV (Y1000) was dissolved in DCM at 45 °C, after which MA (10 wt%) and BPO (0.3 wt%) were added as monomer and initiator, respectively. The mixture was allowed to react for 6 h. The resulting product was purified by Soxhlet extraction with acetone for 48 h to remove unreacted monomers and by-products. The synthesis of IA- and AA-grafted PHBV followed the same procedure. The grafting percentage of MA-*g*-PHBV, AA-*g*-PHBV and IA-*g*-PHBV was determined using titration method, and the result was 1.1 wt%, 0.9 wt% and 0.5 wt % respectively.

2.2.2. Bamboo flour delignification and modification

For delignification, 40 g of bamboo flour was suspended in 1300 mL of deionised water. Sodium chlorite (12 g) and glacial acetic acid (10 mL) were then added, and the mixture was maintained at 80 °C in an oil bath for 1 h. The same quantity of sodium chlorite and acetic acid was added four additional times at hourly intervals. After completion, the flour was repeatedly washed with deionised water under vacuum filtration until a neutral pH was achieved, then oven-dried at 105 °C for 24 h to obtain delignified bamboo flour (DBF). The lignin content of untreated bamboo flour (BF) and DBF was determined according to NREL/TP−510–42168.

For surface modification, 3.6 g of the synthesised coupling agent (i.e. MA-*g*-PHBV, AA-*g*-PHBV and IA-*g*-PHBV) was dissolved in DCM, and 40 g of DBF was added. The mixture was ultrasonicated for 30 min to achieve uniform dispersion. The solvent was then removed under vacuum until nearly dry, and the resulting modified bamboo flour was oven-dried at 60 °C.

2.2.3. Composite preparation

The components were compounded according to the formulation shown in Table 1. Melt blending was performed in a laboratorial internal twin-screw mixer at 180 °C for 10 min. The blends were ground using a plastic grinder and subsequently compression-moulded at 180 °C under 10 MPa using a hot press (Fig. 2). The resulting composites were designated based on the flour type and surface treatment, including BC (BF/PHBV composite), DC (DBF/PHBV composite), MDC (MA-*g*-PHBV modified DBF/PHBV composite), ADC (AA-*g*-PHBV modified DBF/PHBV composite), and IDC (IA-*g*-PHBV modified DBF/PHBV composite).

2.3. Characterisation of bamboo flour and composites

2.3.1. Nuclear magnetic resonance (NMR)

The ^{13}C NMR spectra of the coupling agents were acquired using a Bruker AVANCE III HD 500 spectrometer (Bruker, Germany). Samples were dissolved in deuterated chloroform ($CDCl_3$) prior to analysis. Spectra were recorded with 1024 scans and a relaxation delay of 2 s.

2.3.2. X-ray diffraction (XRD) analysis

XRD analysis was performed on a Rigaku Ultima IV diffractometer equipped with a Cu Kα radiation source (λ=0.15406 nm). Measurements were conducted at 40 kV and 30 mA, scanning from 10° to 40° at a rate of 2 °/min. The relative crystallinity index (*CrI*) of BF and DBF was calculated using the Segal method:

$$\text{Crystallinity Index}(\%) = (I_{002} - I_{am})/I_{002} \times 100\%$$

where I_{002} is the diffraction intensity of the cellulose crystal plane (002) and I_{am} is the scattering intensity at the 2θ of 18°.

2.3.3. Fourier transform infrared (FTIR) analysis

FTIR spectra were recorded using the KBr pellet technique on a Thermo Scientific Nicolet 6700 spectrometer (Thermo Fisher Scientific, USA). Each spectrum was collected over 32 scans at a resolution of 4 cm^{-1}.

2.3.4. Nitrogen adsorption measurements

Nitrogen adsorption-desorption isotherms of untreated and modified bamboo flour were obtained using an ASAP 2460 surface area and pore size analyser (Micromeritics, USA) at 77 K (liquid nitrogen temperature). The pore size distribution was determined using a density functional theory (DFT) model.

2.3.5. Scanning electron microscopy (SEM)

The surface morphology of bamboo flour (before and after modification) and the fracture surfaces of composites after tensile tests were observed using a Hitachi SU8020 field-emission scanning electron microscope (Hitachi, Japan) operated at 3 kV. All samples were oven-dried and coated with a thin layer of gold prior to imaging.

2.3.6. Mechanical property testing

The tensile and flexural properties of the composite materials were tested in accordance with ASTM D638 and ASTM D790 (three-point bending method), respectively. All mechanical tests were conducted on a Universal Testing Machine (SUNS, China), with the crosshead speed at 5 mm/min for tensile test and the loading rate at 2 mm/min for flexural test. All tests were conducted at 23 ± 2°C and 50 ± 5% relative humidity. For each sample, the tensile and flexural property reported is the average of six measurements. The tensile and flexural strengths of PHBV were also measure and given for reference: tensile strength 30.6 ± 1.8 MPa, flexural strength 63.7 ± 0.3 MPa.

2.3.7. Dynamic mechanical analysis (DMA)

Dynamic mechanical properties were characterised using a Q800 dynamic mechanical analyser (TA Instruments, USA) in single cantilever mode. Tests were performed with a strain-controlled configuration, a vibration amplitude of 20 μm and a frequency of 1 Hz. Samples (35 mm × 7.0 mm × 4.0 mm) were heated from 30 °C to 150 °C at a rate of 3 °C/min.

2.3.8. Thermogravimetric analysis (TGA)

Thermal stability was evaluated using an EXSTAR TG/DTA 6300 thermogravimetric analyser (Seiko Instruments, Tokyo, Japan). Samples (5–15 mg) were placed in aluminum crucibles and heated from room temperature to 900 °C under nitrogen at a rate of 10 °C/min.

2.3.9. Differential scanning calorimetry (DSC)

The melting and crystallisation behaviour of the composites were

Table 1
Formulation of composites.

Sample	PHBV (wt%)	BF (wt%)	DBF (wt%)	MA-*g*-PHBV (wt%)	AA-*g*-PHBV (wt%)	IA-*g*-PHBV (wt%)	Lubricant (wt%)	Initiator (wt%)
BC	47	50	0	0	0	0	3	0
DC	47	0	50	0	0	0	3	0
MDC	42	0	50	4.5	0	0	3	0.5
ADC	42	0	50	0	4.5	0	3	0.5
IDC	42	0	50	0	0	4.5	3	0.5

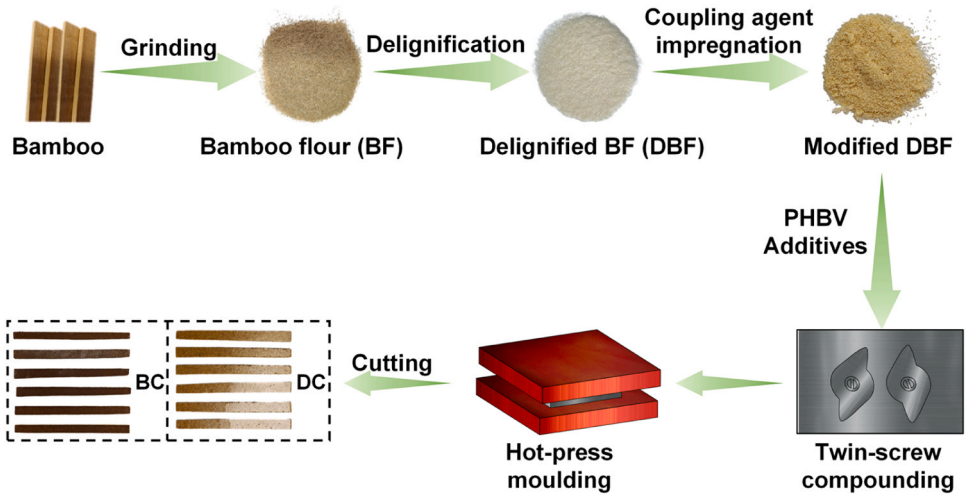

Fig. 2. Preparation procedure of composites.

measured using a NETZSCH DSC 3500 Sirius differential scanning calorimeter (NETZSCH, Germany). Approximately 8–10 mg of each sample was put in an aluminium crucible and analysed under a nitrogen atmosphere. The sample was heated at a rate of 10 °C/min to 200 °C, held at this temperature for 2 min, then cooled to −80 °C before being reheated at 10 °C/min to 200 °C.

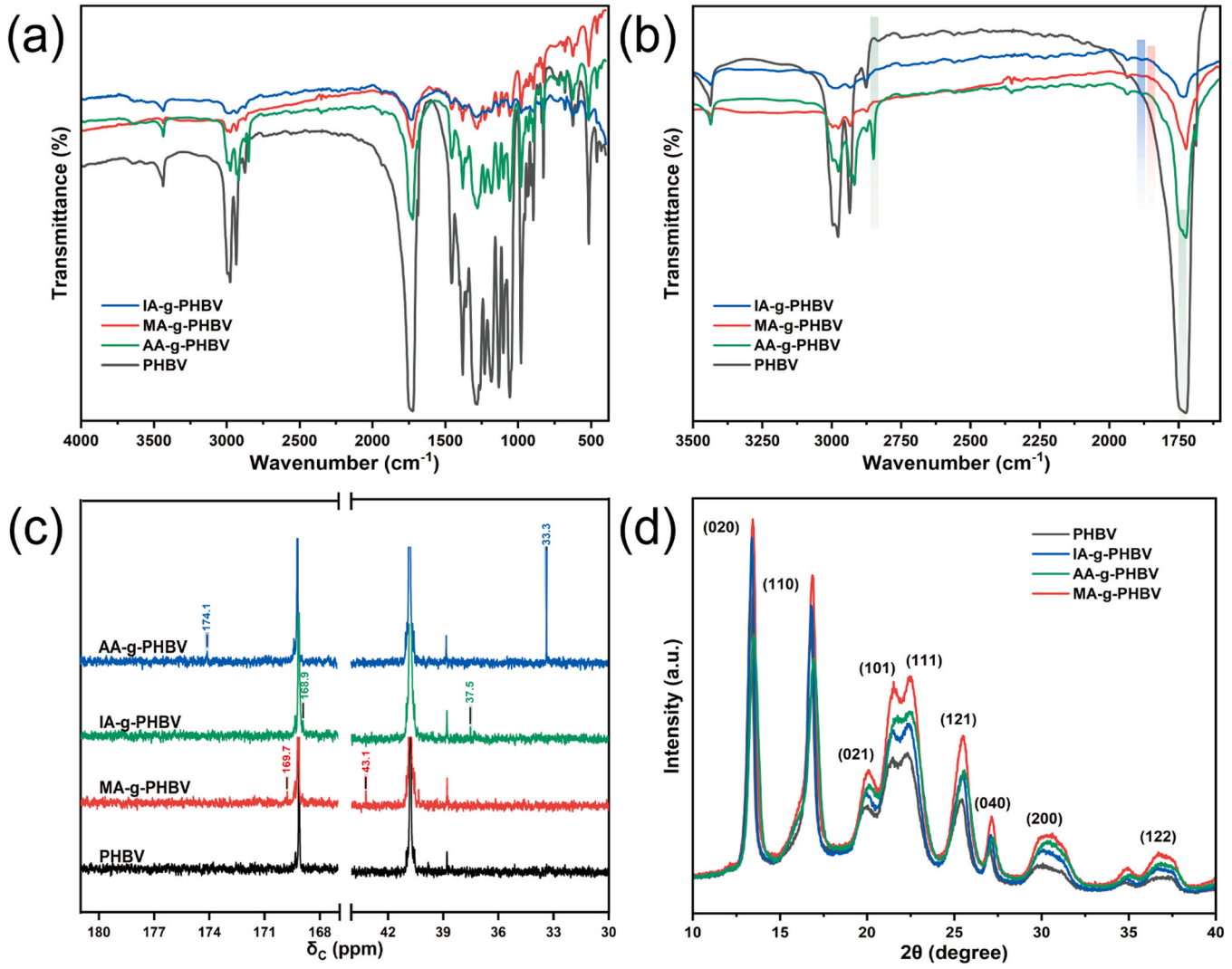

Fig. 3. FTIR spectra at wavenumber 4000–500 cm^{-1} (a), FTIR spectra at wavenumber 3500–1600 cm^{-1} , liquid ^{1} ^{3}C NMR spectra (c) and XRD profiles (d) of PHBV and PHBV-based coupling agents.

3. Results and analysis

3.1. Structure analysis of PHBV-based coupling agents

Figs. 3a and 3b present the FTIR spectra of PHBV and PHBV based coupling agents. The spectra of MA-*g*-PHBV and IA-*g*-PHBV display new absorption peaks at around 1850 cm^{-1} which are assigned to C═O asymmetric stretching of anhydride groups, confirming the successful grafting of both MA and IA onto the PHBV backbone (Ma et al., 2014). The absorption peaks assigning to C═O symmetric stretching should have overlapped with the intrinsic C═O stretching peak of PHBV at 1750 cm^{-1} (Liu et al., 2017). In the case of AA-*g*-PHBV, two new peaks are observed near 1730 cm^{-1} and 2850 cm^{-1} , which are attributed to the C═O stretching vibration and -CH_2 symmetric stretching of AA, respectively (Xie et al., 2024). These spectral changes collectively indicate that MA, IA, and AA were successfully grafted onto PHBV. The grafting percentage of MA-*g*-PHBV, AA-*g*-PHBV and IA-*g*-PHBV was 1.1 wt%, 0.9 wt% and 0.5 wt% respectively from titration determination.^{13}C NMR analysis was also conducted to further explore the grafting reactions and the results were shown in Fig. 3c. The ^{13}C NMR spectrum of AA-*g*-PHBV exhibited new resonances at 174.1 ppm (C═O) and 33.3 ppm, whereas MA-*g*-PHBV showed peaks at 169.7 ppm (C═O) and 43.1 ppm, and IA-*g*-PHBV exhibited peaks at 168.9 ppm (C═O) and 37.5 ppm (Wu, 2014, 2013). These newly appearing chemical shifts are consistent with the FTIR results, suggesting the possible covalent bonds formed between the C═C groups of MA, IA or AA and PHBV macromolecules as shown in Fig. 1a.

XRD patterns of PHBV and the coupling agents are shown in Fig. 3d. Pure PHBV exhibits sharp diffraction peaks at 13.4° and 16.8°, corresponding to the (020) and (110) crystal planes, respectively (Remila et al., 2024a). Additional peaks at 19.8°, 21.3°, 22.4°, 25.4°, 27.0°, 30.0°, and 36.7° are indexed to the (021), (101), (111), (121), (040), (200), and (122) planes of PHBV (De Souza et al., 2023). The presence of peaks at 13.3°, 16.8°, and 22.4° confirms that PHBV primarily adopts an α-type crystalline structure, with a minor β-type phase indicated by the peak at 19.8°. Comparison of PHBV and grafted PHBV shows that the grafting process does not significantly shift the diffraction angles or alter the crystal structure. However, consistent with literature reports (Al et al., 2024; Chen et al., 2003), the diffraction intensities are evidently enhanced in the coupling agents, suggesting improved crystallinity despite the relatively low grafting density.

3.2. Structural analysis of modified bamboo flour

Fig. 4a shows the FTIR spectra of BF and DBF. The peaks at 1425 cm^{-1} and 1510 cm^{-1} , corresponding to the bending and stretching vibrations of lignin's aromatic skeleton, disappear after sodium chlorite treatment, confirming effective delignification. However, the peak near

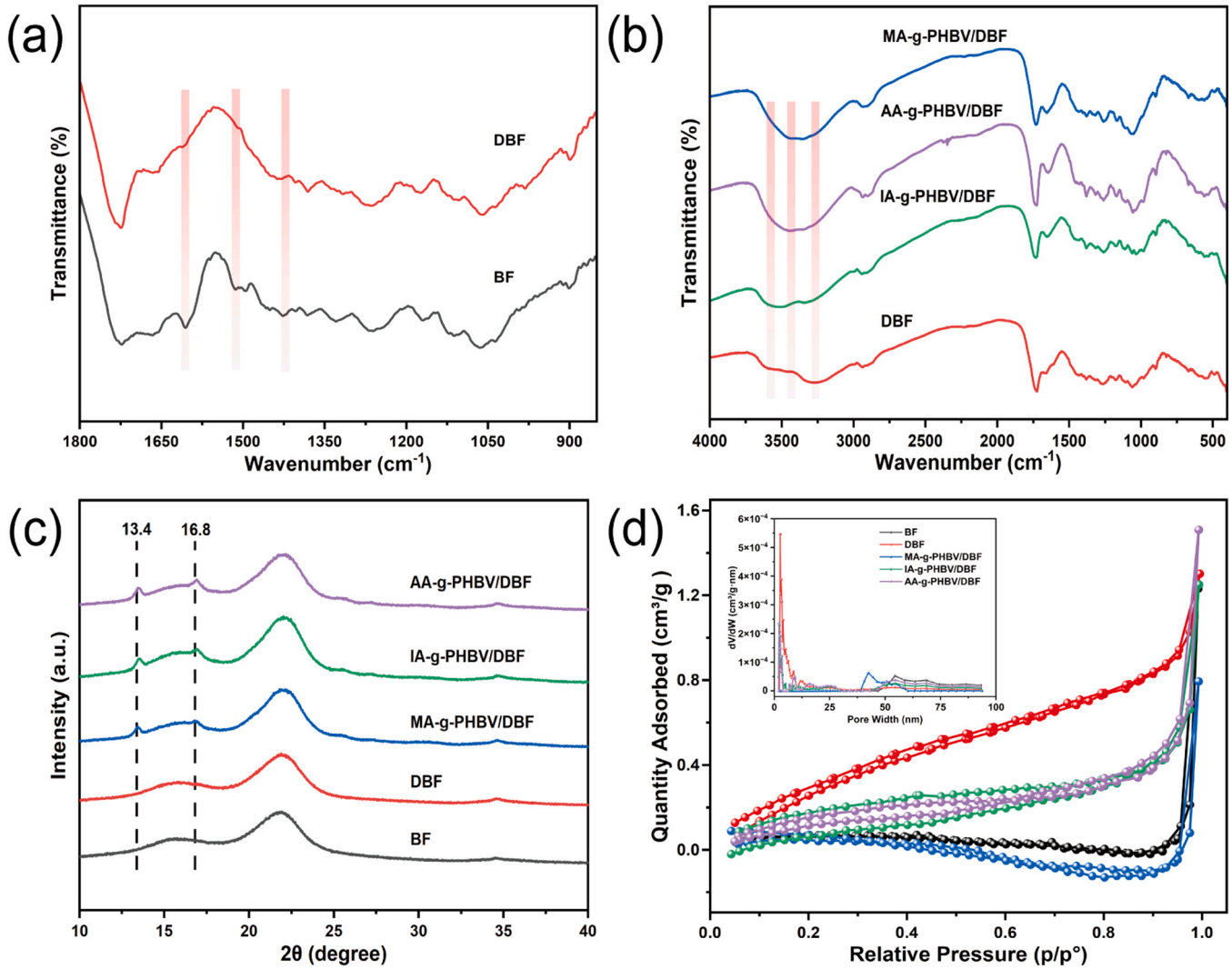

Fig. 4. FTIR spectra at wavenumber 1800–825 cm^{-1} (a), FTIR spectra at wavenumber 4000–400 cm^{-1} , XRD profiles (c) and BET curves (d) of unmodified and modified bamboo flour.

1610 cm^{-1} persists, indicating the presence of a small amount of residual lignin in DBF (Ou et al., 2014a). The lignin content of untreated bamboo flour (BF) and DBF was determined according to NREL/TP−510–42168, and it was 25.26% in BF and 4.79% in DBF, corroborating the FTIR spectral variation due to lignin removal. Fig. 4b compares the FTIR spectra of unmodified and coupling agent-modified DBF. DBF exhibits characteristic peaks at 3250 cm^{-1} and 3580 cm^{-1}, corresponding to strongly hydrogen-bonded -OH groups and free -OH groups, respectively. After impregnation with IA-*g*-PHBV, the 3250 cm^{-1} peak becomes narrower and weaker, while the 3580 cm^{-1} peak broadens and intensifies, indicating a reduction in hydrogen bonding among hydroxyl groups (Wu et al., 2017; Wu, 2013). DBF treated with MA-*g*-PHBV or AA-*g*-PHBV shows an even greater decrease in hydrogen bonding, as evidenced by the merging of the two peaks into a single broad absorption near 3420 cm^{-1}. XRD analysis revealed that delignification increased the crystallinity index of bamboo flour from 51.2% (BF) to 56.7% (DBF), which should be mainly attributed to the removal of lignin and hemicellulose rather than enhanced crystallization or integrity of cellulose. Coupling agent modification did not change the crystal structure of DBF but resulted in diffraction peaks at 13.4° and 16.8°, corresponding to the (020) and (110) planes of PHBV (Fig. 4c), confirming the successful introduction of the PHBV-based coupling agents onto the fibre surface. The chemical structure and crystalline structure results suggest that the coupling agent treatments made the bamboo

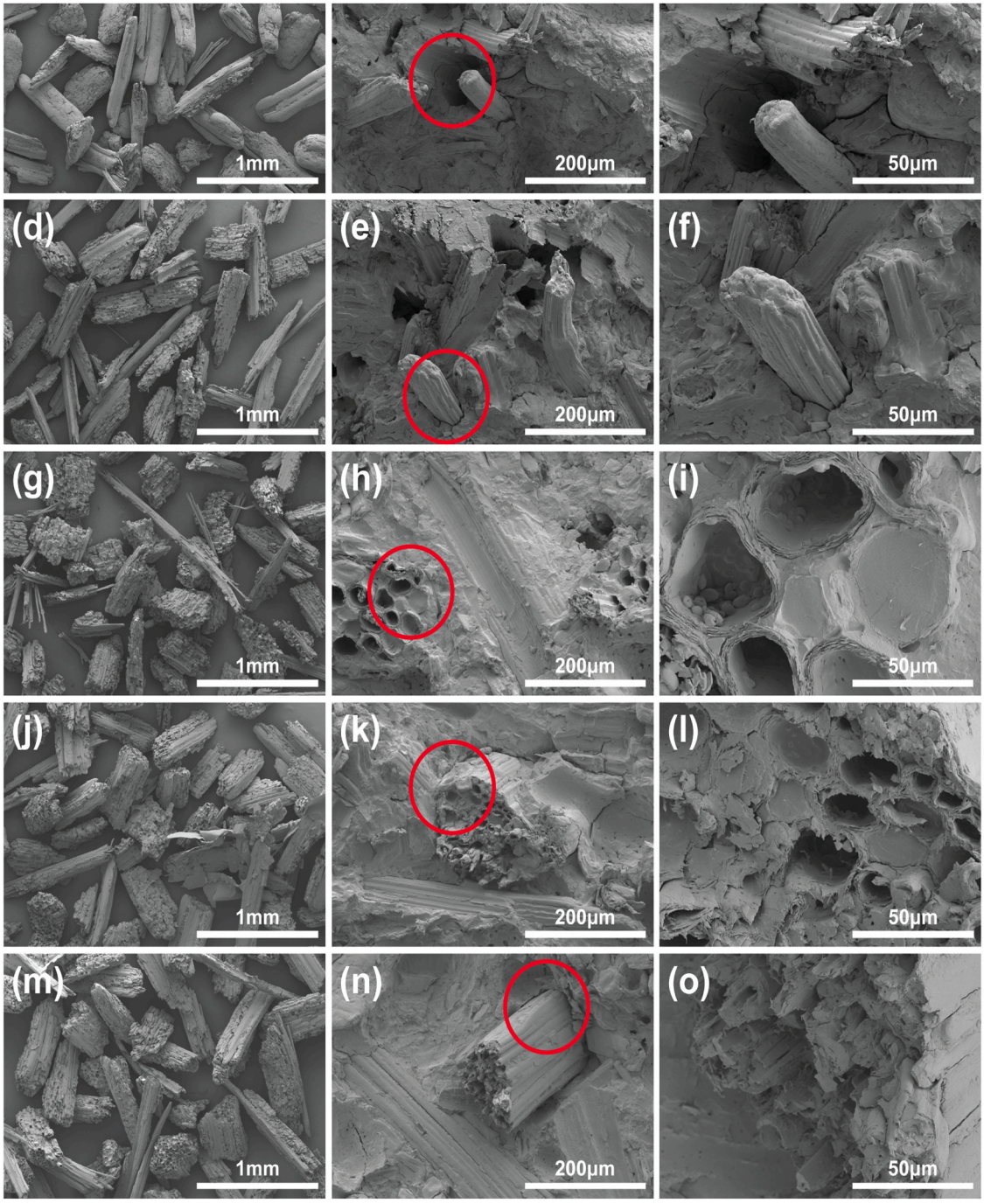

Fig. 5. Microstructural morphology of bamboo flour and tensile fracture surfaces of the composites: (a) BF, (b) and (c) BC, (d) DBF, (e) and (f) DC, (g) MA-*g*-PHBV modified DBF, (h) and (i) MDC, (j)AA-*g*-PHBV modified DBF, (k) and (l) ADC, (m) IA-*g*-PHBV modified DBF, (n) and (o) IDC.

flour more hydrophobic, which should be beneficial to their bonding with PHBV matrix in the composites. Furthermore, the formulation design of this study presents several limitations, i.e. the individual contribution of the impregnation process, coupling agent grafting, and DCP-induced side reactions to the potential interfacial improvement remains unclear, which should be addressed in future work. Specifically, DBF should be subjected to DCM-ultrasonication-vacuum filtration-oven drying process without coupling agent, in order to verify that the impregnation process itself does not modify the bamboo flour surface or morphology; DBF should be impregnated with non-grafted PHBV to distinguish chemical compatibilisation from possible effects caused by physical PHBV deposition, pore filling, improved wetting or changes in flour dispersion; and DBF should be directly compounded with coupling agent to compare with pre-impregnated DBF; and a with/without DCP comparison should be included to isolate the effect of DCP-induced side reactions from coupling agent grafting.

Fig. 4d presents the nitrogen adsorption-desorption isotherms and pore size distributions of BF, DBF and coupling agent modified DBF. For all samples, the adsorption and desorption branches nearly overlap when the relative vapour pressure (P/P_0) is below 0.9. At $P/P_0 > 0.9$, a distinct hysteresis loop appears, signifying capillary condensation within mesopores. According to IUPAC classification, the isotherms lie between Type II and Type IV and exhibit an H3-type hysteresis loop, which is characteristic of slit-shaped pores (Yin et al., 2017, 2015; Ren et al., 2023). This suggests that the overall pore type of bamboo flour remains unchanged after lignin removal and coupling agent impregnation. The pore size distribution curves reveal that delignification significantly increases the volume of mesopores in the 2–10 nm range, indicating that lignin removal primarily affects smaller mesopores (Ren et al., 2023). Conversely, coupling agent treatment reduces the mesopore volume within this range, which may be attributed to partial pore filling by the coupling agent during the impregnation process.

3.3. Microstructure of bamboo flour and composites

The microstructure of BF and modified BF (Fig. 5) show that delignification pretreatment does not produce noticeable internal voids within the bamboo flour. However, it increases surface roughness of the flour as shown Fig. 5a and Fig. 5d, most probably because the lignin that primarily located in the middle lamella and cell corners is removed during treatment, exposing cellulose-rich microfibrils and forming narrow slit-like pores. Although BET analysis confirms that a portion of the dissolved coupling agent solution penetrated into the pores, particularly those in the 2–10 nm range, the penetration phenomenon is not evident in the microstructure. Fig. 5 also shows the tensile fracture surfaces of the five composite materials. In BC (composite with untreated BF), numerous gaps and voids are visible between bamboo flour and matrix, with holes appearing where bamboo flour has been pulled out. This indicates poor interfacial adhesion, which facilitates interfacial debonding and stress concentration, resulting in premature composite failure. In DC (composite with delignified BF), fewer gaps are observed, and bamboo flour pull-out is less pronounced. Delignification appears to enhance deformability of bamboo flour, allowing better conformation to the PHBV matrix during processing, thereby improving interlocking and interfacial adhesion. The composites containing coupling agent modified bamboo flour (MDC, ADC and IDC) exhibit better interfacial bonding by showing fractured bamboo flour, reduced interfacial gaps and fewer cavities left by bamboo flour pull-out after the tensile test.

3.4. Mechanical properties of composites

Figs. 6a and 6b present the flexural and tensile properties of the composites, respectively. Compared with BC, DC shows significant enhancements in tensile strength (+175.8%), tensile modulus (+33.1%), flexural strength (+117.0%), and flexural modulus (+26.7%). These improvements might be attributed to the removal of lignin, which increases the porosity and flexibility of the cell wall of bamboo flour, allowing greater deformation. This enhanced deformability lowers the melt viscosity of the composite (Ou et al., 2014a), improves filler dispersion during blending, and results in better stress transfer within the matrix. In contrast, BC exhibits poor mechanical performance due to weak interfacial bonding as shown in its microstructure, which creates stress concentrations around rigid, poorly dispersed bamboo flour. Short bamboo flour agglomerates act as defect sites that initiate crack propagation (Vandi et al., 2019), ultimately leading to premature failure. It should be pointed out that although DC suggested higher mechanical

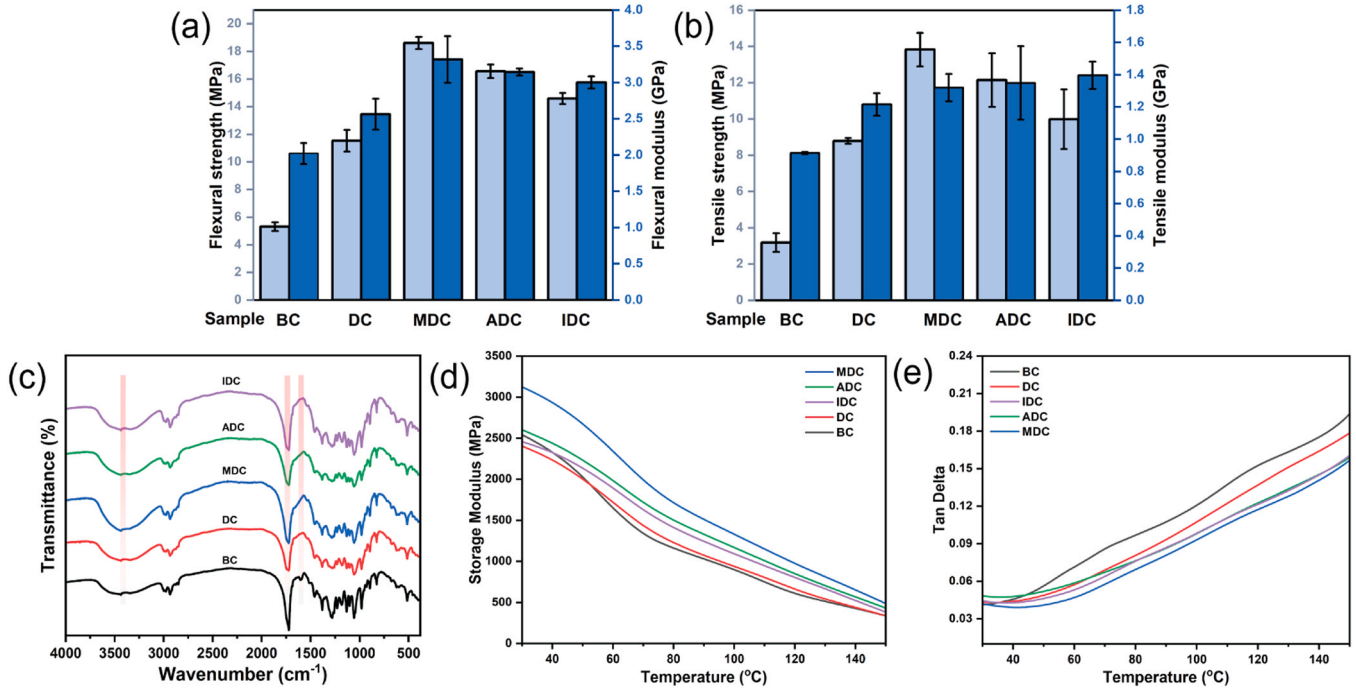

Fig. 6. Flexural property (a), tensile property (b), FTIR spectra (c), storage modulus (d) and Tanδ(e) of the composites.

properties, the potential trade-off between lignin/hemicellulose removal and cellulose degradation were unclear, which are worth exploration in future study.

Further improvements are observed in MDC, ADC, and IDC, with MDC achieving the most pronounced enhancements. The tensile strength of MDC increases by 57.1% relative to DC, reaching 13.8 MPa, while its flexural strength rises by 61.4% to 18.6 MPa. These improvements are primarily due to coupling agent treatment, which reduces hydrogen bonding between hydroxyl groups of DBF (Fig. 4b), promoting better dispersion of bamboo flour in PHBV matrix. The increased intensity of the hydroxyl peak near 3430 cm^{-1} (Fig. 6c) suggests the formation of new hydrogen bonds between -OH groups of DBF and -COOH of PHBV, further strengthening interfacial adhesion. Moreover, a portion of the coupling agent infiltrates the pores formed by lignin removal, reinforcing DBF while maintaining its plasticity. The intensity at 1730 cm^{-1} (C═O) has increased, which should be ascribed to the introduction of carbonyl-containing moieties in the coupling agent and also potential interactions between the coupling agent and DBF (Xu et al., 2021; Zhou et al., 2021), while PHBV chains might crosslink with the polymeric backbone of coupling agent. These possible chemical interactions may have enhanced interfacial adhesion and contributed to the improved mechanical properties of the composite. Although ADC exhibits slightly lower mechanical performance than MDC, its tensile and flexural strengths still reach 12.1 MPa and 16.5 MPa, respectively. In contrast, IDC shows a lower tensile strength (9.9 MPa), which is likely due to the relatively low grafting rate of IA-*g*-PHBV (0.5 wt%) compared with MA-*g*-PHBV and AA-*g*-PHBV (0.9–1.1 wt%) under the same reaction conditions. This discrepancy can be attributed to the slower reactivity of IA, leading to reduced grafting efficiency (Ku Marsilla and Verbeek, 2015). It is noteworthy that although DCP acts as an initiator to promote interfacial bonding between the coupling agent and the PHBV matrix (Fei et al., 2004), its nature is to induce competitive reactions while facilitating crosslinking, and it could also lead to chain scission or branching. The lack of DCP in BC and DC makes it difficult to isolate the contribution of coupling agent from the possible effect of DCP-induced PHBV degradation, chain scission, branching or crosslinking. Therefore, a control composite with coupling agent but without DCP should be considered in future work.

Shapiro-Wilk and Levene's tests indicated that the assumptions of normality and homogeneity of variance were not violated, the associated ANOVA and Tukey HSD results are presented in Table 2. It is evident that delignification treatment had a significant effect on both tensile and flexural properties. The coupling agent surface treatment significantly influenced the tensile strength, tensile modulus, and flexural strength, while its effect on the flexural modulus was negligible. Table 3 summarises the mechanical properties of PHBV composite filled with ≥ 40 wt% cellulosic fibre/flour, such as spruce, pine, maple, chestnut shell fibre or flour etc. It can be seen that the tensile strength of these composites is in the range of 13–25 MPa depending on the fibre origin, PHBV property, treatment method, processing technique (e.g. extrusion or hot-press compression) etc.

Values marked with the same letter within the same group (Group 1: BC/DC; Group 2: DC/MDC/ADC/IDC) are not significantly different at the 5% significance level based on ANOVA and Tukey's test; no comparison was made between groups.

Table 2
Mechanical properties of the composites and associated statistical analysis.

Sample	BC	DC	MDC	ADC	IDC
Tensile Strength (MPa)	3.1 ± 0.5^{a}	8.8 ± 0.1$^{b/a'}$	13.8 ± 0.9$^{b'}$	12.1 ± 0.1$^{c'}$	9.9 ± 1.6$^{d'}$
Flexural Strength (MPa)	5.3 ± 0.3^{a}	11.5 ± 0.7$^{b/a'}$	18.6 ± 0.4$^{b'}$	16.5 ± 0.4$^{c'}$	14.5 ± 0.4$^{d'}$

Table 3
Comparison of mechanical properties of PHBV composites filled with ≥ 40 wt% cellulosic fibre/flour.

Material Composition (Matrix-Filler)	Flour content (wt%)	Tensile strength (MPa)	Flexural strength (MPa)	Ref.
PHBV-spruce	50	13.9	-	(Dufresne et al., 2003)
PHBV-olive stone	50	13.2	-	
PHBV-maple	40	16.75 ± 0.5	30.0 ± 1	(Chen et al., 2025)
PHBV-corn straw	40	19 ± 0.4	23.2 ± 1.2	(Elsheikh et al., 2022)
PHBV-soy stalk	40	18 ± 0.5	25.3 ± 1.1	
PHBV-wheat straw	40	19.9 ± 0.4	24.3 ± 0.4	
PHBV-pine	40	22.8 ± 1.2	-	(Qiang et al., 2014)
PHBV-chestnut shell	40	~17	-	(Bhattacharjee and Bajwa, 2018)
PHBV-tea plant	40	~20	-	(Jung et al., 2025)
PHBV-pine	45	24.7 ± 0.9	-	(Singh et al., 2023)
PHBV-pine	50	24.8	-	(Chan et al., 2019)
PHBV-bamboo	50	13.8	18.6	This study
Neat PHBV	-	30.6	63.7	This study

Fig. 6d shows the storage modulus of the composites as a function of temperature (30–150 °C). As expected, storage modulus decreases with increasing temperature due to enhanced mobility of PHBV molecular chains. Across most of the temperature range, DC maintains a slightly higher storage modulus than BC, consistent with the increased deformability and better interfacial adhesion of DC, the storage modulus at 30 °C of DC, MDC, ADC, and IDC are 2403 MPa, 3122 MPa, 2603 MPa, and 2458 MPa, respectively. The composites containing coupling agent treated bamboo flour exhibit a further increase in storage modulus compared with DC, reflecting improved constituent compatibility and interfacial adhesion (Remila et al., 2024b). Furthermore, the coupling agent treated composites display lower loss factors (Fig. 6e) than BC and DC, indicating restricted molecular chain motion near the interface due to strong flour-matrix adhesion (Ou et al., 2014b). As the temperature increases, the tanδ increases more significantly for BC and DC than for MDC, ADC and IDC. This further confirms that the combination of delignification and coupling agent impregnation could enhance stress transfer efficiency at the bamboo flour-matrix interface, leading the composite material to favour elastic energy storage over viscous dissipation during deformation. The higher storage modulus combined with a lower loss factor suggests that MA-*g*-PHBV modified bamboo flour provides the composite with the strongest interfacial bonding and most efficient stress transfer.

3.5. Thermal properties of composites

Figs. 7a and 7b present differential scanning calorimetry (DSC) results of the composites. It was observed that the crystallisation temperature (T_c) decreases from 111.74 °C in BC to 107.29 °C in DC, and the composites modified with coupling agent impregnation (MDC, ADC, IDC) show slightly higher T_c values than DC (Table 4). In addition, the crystallisation peak intensity of DC, MDC, ADC, and IDC is higher than that of BC (Fig. 7a). The improved plasticity of DBF resulted from delignification could benefit PHBV chain mobility and lower the energy barrier for crystallisation, while the coupling agent treatments restrict molecular chain motion, leading to a slightly higher T_c in MDC, ADC and IDC than DC. These results are consistent with the above dynamic mechanical analysis.

All composites (DC, MDC, ADC, IDC) display two melting peaks, which appeared at lower temperatures than that of BC. The lower-temperature peak corresponds to the melting crystals of low integrity and thinner layered structures, while the higher temperature peak are associated with the melting of more complete crystals (Malmir et al.,

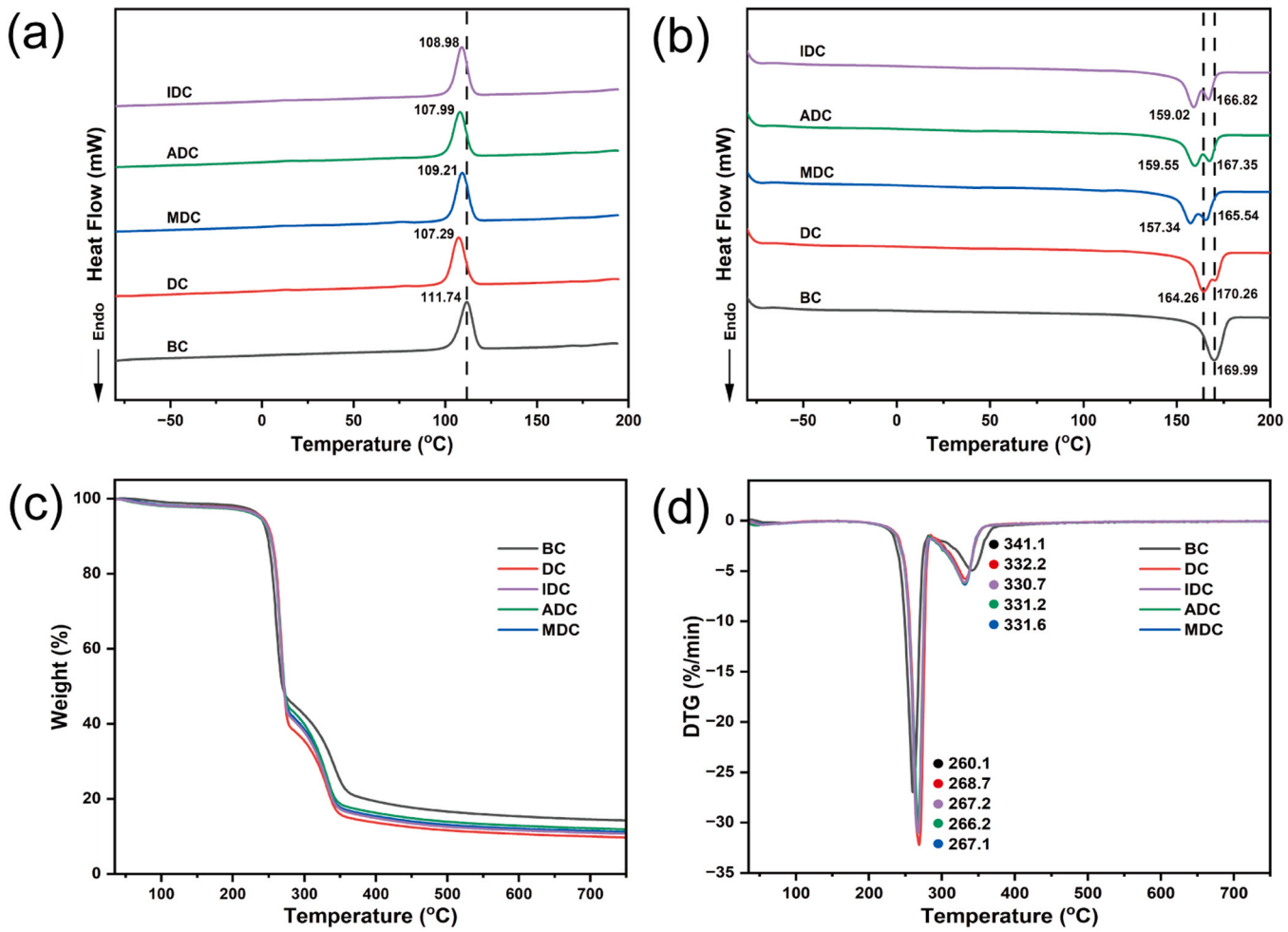

Fig. 7. DSC cooling curves (a), DSC heating curves (b), TG curves (c) and DTG curves (d) of the composites.

Table 4
T_c and T_m values for the composites.

Sample	T_c (°C)	T_{m1} (°C)	T_{m2} (°C)
BC	111.74	169.99	-
DC	107.29	164.26	170.26
MDC	109.21	157.34	165.54
ADC	107.99	159.55	167.35
IDC	108.98	159.02	166.82

2019). DBF exhibits a more pronounced inducing effect on the heterogeneous nucleation of PHBV in comparison to BF, thereby enhancing its crystallisation rate. This process leads to the formation of smaller crystals and the generation of a low-temperature melting peak (Malmir et al., 2017). The introduction of MA, AA, and IA groups in MDC, ADC, and IDC has the potential to disrupt the regularity of the PHBV molecular chain, thereby reducing the activation energy required for composite melting. This results in a shift of both melting peaks of the composites to lower temperatures (Remila et al., 2024a; Yao et al., 2025).

Figs. 7c and 7d present the thermogravimetric (TG) and derivative thermogravimetric (DTG) curves of composites. The thermal degradation process of all samples can be divided into three distinct stages. The initial stage (220–280 °C) is characterised by the degradation of hemicellulose, with the PHBV matrix undergoing continuous decomposition within this temperature range. The subsequent stage (280–380 °C) involves cellulose degradation, accompanied by further decomposition of the PHBV matrix. The third stage (380–700 °C) is characterised by the slow carbonisation of lignin (Öner et al., 2018; Yang et al., 2006). Following lignin removal, the maximum degradation temperature of cellulose decreased from 340 °C to approximately 330 °C, reflecting the loss of lignin's protective effect during thermal decomposition (Zhu and Du, 2024). As with DC, the T_{max2} for MDC, IDC and ADC are marginally lower than those for BC. Nevertheless, the T_{max1} of MDC, ADC, and IDC exceeds that of BC, which may be associated with improved interfacial compatibility and the presence of coupling agents, although direct evidence is needed to confirm covalent bonding. The residual char yield at 700 °C was significantly lower in composites containing delignified bamboo flour. BC exhibited a residue rate of 14.42%, whereas DC, MDC, ADC, and IDC showed reduced residue rates of 8.86%, 10.46%, 11.09%, and 9.86%, respectively. This reduction is consistent with the lower lignin content, as char residues mainly originate from lignin carbonisation.

4. Conclusion

High-loading bamboo flour/PHBV biocomposites with enhanced interfacial bonding were successfully prepared by applying a synergistic treatment via delignification of bamboo flour and impregnation of PHBV-based coupling agents. The results suggest that the increased surface roughness and deformability of the treated bamboo flour might promote mechanical interlocking with the matrix, while the PHBV-based coupling agents improved interfacial compatibility by reducing flour agglomeration, enhancing wetting, and enabling possible chemical interactions between functional groups. The tensile strength of MDC (13.8 MPa), ADC (12.1 MPa) and IDC (9.9 MPa) was increased by

333.3%, 280.8% and 213.1% respectively, and their flexural strength (18.6 MPa for MDC, 16.5 MPa for ADC and 14.5 MPa for IDC) was increased by 250.4%, 211.8% and 174.6% respectively. The synergistic treatment resulted in a better interfacial bonding by showing fractured bamboo flour, reduced interfacial gaps and fewer cavities on the fracture surface of the composites. These findings demonstrate that the synergistic modification strategy is an effective approach to enhance interfacial compatibility and mechanical robustness of high fibre loading and fully biodegradable natural fibre composites.

CRediT authorship contribution statement

Mizi Fan: Writing – review & editing. **Yonghui Zhou:** Writing – review & editing, Supervision, Project administration. **Jiangtao Xu:** Visualization, Validation. **Chuanshuang Hu:** Writing – review & editing, Supervision, Project administration. **Xiaolu Wu:** Validation, Formal analysis. **Kun Liu:** Investigation, Formal analysis. **Lanying Lin:** Writing – review & editing, Methodology. **Nuoyan Ou:** Investigation, Data curation. **Zhuoyu Lu:** Writing – original draft, Methodology, Formal analysis, Data curation.

Declaration of Competing Interest

The authors declare that they have no known competing financial interests or personal relationships that could have appeared to influence the work reported in this paper.

Acknowledgements

The authors gratefully acknowledge the funding from the National Natural Science Foundation of China (32572163) and Natural Science Foundation of Guangdong Province (2026A1515011599).

Data availability

Data will be made available on request.

References

Al, G., Aydemir, D., Altuntaş, E., 2024. The effects of PHB-g-MA types on the mechanical, thermal, morphological, structural, and rheological properties of polyhydroxybutyrate biopolymers. Int. J. Biol. Macromol. 264, 130745. https://doi.org/10.1016/j.ijbiomac.2024.130745.

Bhattacharjee, S., Bajwa, D.S., 2018. Degradation in the mechanical and thermo-mechanical properties of natural fiber filled polymer composites due to recycling. Constr. Build. Mater. 172, 1–9. https://doi.org/10.1016/j.conbuildmat.2018.03.010.

Burgstaller, C., Renner, K., 2023. Recycling of Wood–Plastic Composites—A Reprocessing Study. Macromol 3, 754–765. https://doi.org/10.3390/macromol3040043.

Chan, C.M., Vandi, L.-J., Pratt, S., Halley, P., Ma, Y., Chen, G.-Q., et al., 2019. Understanding the effect of copolymer content on the processability and mechanical properties of polyhydroxyalkanoate (PHA)/wood composites. Composites Part A Applied Science Manufacturing 124, 105437. https://doi.org/10.1016/j.compositesa.2019.05.005.

Chen, L., Gao, F., Liu, J., Li, D., Chen, D., Li, Y., et al., 2025. Enhancing wood-plastic composites for high-performance structural applications. Composites Part B Engineering 299, 112410. https://doi.org/10.1016/j.compositesb.2025.112410.

Chen, C., Peng, S., Fei, B., Zhuang, Y., Dong, L., Feng, Z., et al., 2003. Synthesis and characterization of maleated poly(3-hydroxybutyrate). J. Appl. Polym. Sci. 88, 659–668. https://doi.org/10.1002/app.11771.

Conti Silva, J.A., Walton, H., Dever, S., Kardel, K., Martins Lacerda, T., Lopes Quirino, R., 2022. Itaconic Anhydride as a Green Compatibilizer in Composites Prepared by the Reinforcement of a Tung Oil-Based Thermosetting Resin with Miscanthus, Pine Wood, or Algae Biomass. Coatings 13, 25. https://doi.org/10.3390/coatings13010025.

De Souza, M.F., Luna, C.B.B., Siqueira, D.D., Bezerra, E.D.O.T., De Cerqueira, G.R., Araújo, E.M., et al., 2023. Toward the Improvement of Maleic Anhydride Functionalization in Polyhydroxybutyrate (PHB): Effect of Styrene Monomer and Sn (Oct)2 Catalyst. IJMS 24, 14409. https://doi.org/10.3390/ijms241914409.

Dufresne, A., Dupeyre, D., Paillet, M., 2003. Lignocellulosic flour-reinforced poly (hydroxybutyrate-co-valerate) composites. J. Appl. Polym. Sci. 87, 1302–1315. https://doi.org/10.1002/app.11546.

Elsheikh, A.H., Panchal, H., Shanmugan, S., Muthuramalingam, T., El-Kassas, AhmedM., Ramesh, B., 2022. Recent progresses in wood-plastic composites: Pre-processing treatments, manufacturing techniques, recyclability and eco-friendly assessment. Clean. Eng. Technol. 8, 100450. https://doi.org/10.1016/j.clet.2022.100450.

Farmahini-Farahani, M., Khan, A., Lu, P., Bedane, A.H., Eic, M., Xiao, H., 2017. Surface morphological analysis and water vapor barrier properties of modified Cloisite 30B/poly(3-hydroxybutyrate-co-3-hydroxyvalerate) composites. Appl. Clay Sci. 135, 27–34. https://doi.org/10.1016/j.clay.2016.08.033.

Fei, B., Chen, C., Chen, S., Peng, S., Zhuang, Y., An, Y., et al., 2004. Crosslinking of poly [(3-hydroxybutyrate)- *co* -(3-hydroxyvalerate)] using dicumyl peroxide as initiator. Polym. Int. 53, 937–943. https://doi.org/10.1002/pi.1477.

Frącz, W., Janowski, G., Bąk, 2021. Influence of the Alkali Treatment of Flax and Hemp Fibers on the Properties of PHBV Based Biocomposites. Polymers 13, 1965. https://doi.org/10.3390/polym13121965.

Hao, X., Xu, J., Zhou, H., Tang, W., Li, W., Wang, Q., et al., 2021. Interfacial adhesion mechanisms of ultra-highly filled wood fiber/polyethylene composites using maleic anhydride grafted polyethylene as a compatibilizer. Mater. & Des. 212, 110182. https://doi.org/10.1016/j.matdes.2021.110182.

Hwang, S.W., Lee, S.B., Lee, C.K., Lee, J.Y., Shim, J.K., Selke, S.E.M., et al., 2012. Grafting of maleic anhydride on poly(L-lactic acid). Effects on physical and mechanical properties. Polym. Test. 31, 333–344. https://doi.org/10.1016/j.polymertesting.2011.12.005.

Jung, S., Bang, J., Kim, J., Lim, H., Kim, S., Choi, I.-G., et al., 2025. Hierarchical interfacial engineering of lyocell fiber/polybutylene succinate composites for robust biodegradable natural fiber–reinforced plastics. Composites Part B Engineering 296, 112253. https://doi.org/10.1016/j.compositesb.2025.112253.

Ku Marsilla, K.I., Verbeek, C.J.R., 2015. Modification of poly(lactic acid) using itaconic anhydride by reactive extrusion. Eur. Polym. J. 67, 213–223. https://doi.org/10.1016/j.eurpolymj.2015.03.054.

Liu, W., Liu, T., Liu, T., Liu, T., Xin, J., Hiscox, W.C., et al., 2017. Improving Grafting Efficiency of Dicarboxylic Anhydride Monomer on Polylactic Acid by Manipulating Monomer Structure and Using Comonomer and Reducing Agent. Ind. Eng. Chem. Res. 56, 3920–3927. https://doi.org/10.1021/acs.iecr.6b05051.

Ma, P., Cai, X., Lou, X., Dong, W., Chen, M., Lemstra, P.J., 2014. Styrene-assisted melt free-radical grafting of maleic anhydride onto poly(β-hydroxybutyrate). Polym. Degrad. Stab. 100, 93–100. https://doi.org/10.1016/j.polymdegradstab.2013.12.005.

Malmir, S., Montero, B., Rico, M., Barral, L., Bouza, R., 2017. Morphology, thermal and barrier properties of biodegradable films of poly (3-hydroxybutyrate-co-3-hydroxyvalerate) containing cellulose nanocrystals. Composites Part A Applied Science Manufacturing 93, 41–48. https://doi.org/10.1016/j.compositesa.2016.11.011.

Malmir, S., Montero, B., Rico, M., Barral, L., Bouza, R., Farrag, Y., 2019. Novel Self-Reinforced Films Based on Poly (3-Hydroxybutyrate-Co-3-Hydroxyvalerate) (PHBV) and PHBV Microparticles. Polym. Eng. & Sci. 59, E120–E128. https://doi.org/10.1002/pen.24882.

Nath, D., Rodriguez-Uribe, A., Wang, T., Misra, M., Mohanty, A.K., 2025. Green composites from plasticized poly(3-hydroxybutyrate-co-3-hydroxyvalerate) bioplastic and cellulosic fiber: Effect of compatibilizer and grafting percentage on interfacial adhesion and biocomposite performance. Int. J. Biol. Macromol. 315, 144107. https://doi.org/10.1016/j.ijbiomac.2025.144107.

Niwa, S., Saito, Y., Ito, M., Ogoe, S., Ito, H., Sunaga, Y., et al., 2017. Direct spectroscopic detection of binding formation by kneading of biomass filler and acid-modified resin. Polymer 125, 161–171. https://doi.org/10.1016/j.polymer.2017.08.007.

Öner, M., Kızıl, G., Keskin, G., Pochat-Bohatier, C., Bechelany, M., 2018. The Effect of Boron Nitride on the Thermal and Mechanical Properties of Poly(3-hydroxybutyrate-co-3-hydroxyvalerate). Nanomaterials 8, 940. https://doi.org/10.3390/nano8110940.

Ou, R., Xie, Y., Wolcott, M.P., Sui, S., Wang, Q., 2014b. Morphology, mechanical properties, and dimensional stability of wood particle/high density polyethylene composites: Effect of removal of wood cell wall composition. Mater. & Des. 58, 339–345. https://doi.org/10.1016/j.matdes.2014.02.018.

Ou, R., Xie, Y., Wolcott, M.P., Yuan, F., Wang, Q., 2014a. Effect of wood cell wall composition on the rheological properties of wood particle/high density polyethylene composites. Compos. Sci. Technol. 93, 68–75. https://doi.org/10.1016/j.compscitech.2014.01.001.

Qiang, T., Yu, D., Zhang, A., Gao, H., Li, Z., Liu, Z., et al., 2014. Life cycle assessment on polylactide-based wood plastic composites toughened with polyhydroxyalkanoates. J. Clean. Prod. 66, 139–145. https://doi.org/10.1016/j.jclepro.2013.11.074.

Rao, J., Zhou, Y., Fan, M., 2018. Revealing the Interface Structure and Bonding Mechanism of Coupling Agent Treated WPC. Polymers 10, 266. https://doi.org/10.3390/polym10030266.

Remila, B., Zembouai, I., Zaidi, L., Alane, A., Kaci, M., Kervoelen, A., et al., 2024a. Investigations on structure and properties of poly (3-hydroxybutyrate-co-3-hydroxyvalerate) (PHBV) reinforced by diss fibers: Effect of various surface treatments. Ind. Crops Prod. 221, 119302. https://doi.org/10.1016/j.indcrop.2024.119302.

Remila, B., Zembouai, I., Zaidi, L., Alane, A., Yalaoui, K., Kaci, M., et al., 2024b. Effect of PHBV-g-MA compatibilizer on the properties of poly(3-hydroxybutyrate-co-3-hydroxyvalerate)/polylactide blend/Diss fibers biocomposites. J. Polym. Sci. 62, 4587–4598. https://doi.org/10.1002/pol.20240406.

Ren, W., Cao, M., Zhou, Y., Zhu, J., Wang, H., Yu, Y., 2023. Pore structure evolution of bamboo fiber and parenchyma cell wall during sequential chemical removal. Ind. Crops Prod. 193, 116165. https://doi.org/10.1016/j.indcrop.2022.116165.

Singh, M.K., Mohanty, A.K., Misra, M., 2023. Upcycling of waste polyolefins in natural fiber and sustainable filler-based biocomposites: A study on recent developments and

future perspectives. Composites Part B Engineering 263, 110852. https://doi.org/10.1016/j.compositesb.2023.110852.
Vandi, L.-J., Chan, C.M., Werker, A., Richardson, D., Laycock, B., Pratt, S., 2019. Extrusion of wood fibre reinforced poly(hydroxybutyrate-co-hydroxyvalerate) (PHBV) biocomposites: Statistical analysis of the effect of processing conditions on mechanical performance. Polym. Degrad. Stab. 159, 1–14. https://doi.org/10.1016/j.polymdegradstab.2018.10.015.
Wang, T., Xiong, C., Li, P., 2026. Manufacturing strategies for cellulose-based EMI shielding composites: Process-driven microstructures and EMI shielding performance. Composites Part B Engineering 309, 113093. https://doi.org/10.1016/j.compositesb.2025.113093.
Wu, C.-S., 2013. Preparation, characterization and biodegradability of crosslinked tea plant-fibre-reinforced polyhydroxyalkanoate composites. Polym. Degrad. Stab. 98, 1473–1480. https://doi.org/10.1016/j.polymdegradstab.2013.04.013.
Wu, C.-S., 2014. Preparation and Characterization of Polyhydroxyalkanoate Bioplastic-Based Green Renewable Composites from Rice Husk. J. Polym. Environ. 22, 384–392. https://doi.org/10.1007/s10924-014-0662-y.
Wu, C.-S., Liao, H.-T., Cai, Y.-X., 2017. Characterisation, biodegradability and application of palm fibre-reinforced polyhydroxyalkanoate composites. Polym. Degrad. Stab. 140, 55–63. https://doi.org/10.1016/j.polymdegradstab.2017.04.016.
Xie, X., Ling, X., Tian, F., Tang, Z., 2024. Hydrophilicity regulation and microstructure change of Ethylene-tetrafluoroethylene copolymer films grafted acrylic acid by irradiation-induced co-grafting. Colloids Surf. A Physicochem. Eng. Asp. 700, 134755. https://doi.org/10.1016/j.colsurfa.2024.134755.
Xu, J., Hao, X., Tang, W., Zhou, H., Chen, L., Guo, C., et al., 2021. Mechanical properties, morphology, and creep resistance of ultra-highly filled bamboo fiber/polypropylene composites: Effects of filler content and melt flow index of polypropylene. Constr. Build. Mater. 310, 125289. https://doi.org/10.1016/j.conbuildmat.2021.125289.
Yang, H., Yan, R., Chen, H., Zheng, C., Lee, D.H., Liang, D.T., 2006. In-Depth Investigation of Biomass Pyrolysis Based on Three Major Components: Hemicellulose, Cellulose and Lignin. Energy Fuels 20, 388–393. https://doi.org/10.1021/ef0580117.
Yao, X., Xu, Y., Zhu, D., Zhang, Z., Feng, C., Zhu, J., et al., 2025. Bio-based high-grafting-rate compatibilizer: Dynamic reactive extrusion synthesis of itaconic anhydride-based copolymers with polypropylene grafts and the application in plant fiber composites. Ind. Crops Prod. 226, 120619. https://doi.org/10.1016/j.indcrop.2025.120619.
Yin, J., Song, K., Lu, Y., Zhao, G., Yin, Y., 2015. Comparison of changes in micropores and mesopores in the wood cell walls of sapwood and heartwood. Wood Sci. Technol. 49, 987–1001. https://doi.org/10.1007/s00226-015-0741-9.
Yin, J., Yuan, T., Lu, Y., Song, K., Li, H., Zhao, G., et al., 2017. Effect of compression combined with steam treatment on the porosity, chemical compositon and cellulose crystalline structure of wood cell walls. Carbohydr. Polym. 155, 163–172. https://doi.org/10.1016/j.carbpol.2016.08.013.
Zhang, W., Yao, X., Khanal, S., Xu, S., 2018. A novel surface treatment for bamboo flour and its effect on the dimensional stability and mechanical properties of high density polyethylene/bamboo flour composites. Constr. Build. Mater. 186, 1220–1227. https://doi.org/10.1016/j.conbuildmat.2018.08.003.
Zhou, Y., Katsou, E., Fan, M., 2021. Interfacial structure and property of eco-friendly carboxymethyl cellulose/poly(3-hydroxybutyrate-co-3-hydroxyvalerate) biocomposites. Int. J. Biol. Macromol. 179, 550–556. https://doi.org/10.1016/j.ijbiomac.2021.03.009.
Zhu, J., Du, C., 2024. Interaction between lignin and cellulose during the pyrolysis process. Int. J. Biol. Macromol. 265, 131093. https://doi.org/10.1016/j.ijbiomac.2024.131093.